Remote Sens. **2013**, *5*, 3331-3356; doi:10.3390/rs5073331

OPEN ACCESS

Remote Sensing

ISSN 2072-4292

www.mdpi.com/journal/remotesensing

Article

A Remote-Sensing Driven Tool for Estimating Crop Stress and Yields

Vikalp Mishra [1], James F. Cruise [1,*], John R. Mecikalski [2], Christopher R. Hain [3] and Martha C. Anderson [4]

[1] Earth Systems Science Center, National Space Science and Technology Center, University of Alabama in Huntsville, 320 Sparkman Drive, Huntsville, AL 35805, USA; E-Mail: mishrav@nsstc.uah.edu

[2] Atmospheric Science Department, University of Alabama in Huntsville, 320 Sparkman Drive, Huntsville, AL 35805, USA; E-Mail: johnm@nsstc.uah.edu

[3] Earth System Science Interdisciplinary Center, University of Maryland-College Park, College Park, MD 20740, USA; E-Mail: christopher.hain@gmail.com

[4] Hydrology and Remote Sensing Laboratory, USDA Agricultural Research Service, Beltsville, MD 20705, USA; E-Mail: martha.anderson@ars.usda.gov

***** Author to whom correspondence should be addressed; E-Mail: james.cruise@nsstc.uah.edu; Tel.: +1-256-961-7659.

Received: 18 May 2013; in revised form: 28 June 2013 / Accepted: 5 July 2013 / Published: 12 July 2013

Abstract: Biophysical crop simulation models are normally forced with precipitation data recorded with either gauges or ground-based radar. However, ground-based recording networks are not available at spatial and temporal scales needed to drive the models at many critical places on earth. An alternative would be to employ satellite-based observations of either precipitation or soil moisture. Satellite observations of precipitation are currently not considered capable of forcing the models with sufficient accuracy for crop yield predictions. However, deduction of soil moisture from space-based platforms is in a more advanced state than are precipitation estimates so that these data may be capable of forcing the models with better accuracy. In this study, a mature two-source energy balance model, the Atmosphere Land Exchange Inverse (ALEXI) model, was used to deduce root zone soil moisture for an area of North Alabama, USA. The soil moisture estimates were used in turn to force the state-of-the-art Decision Support System for Agrotechnology Transfer (DSSAT) crop simulation model. The study area consisted of a mixture of rainfed and irrigated cornfields. The results indicate that the model forced with the ALEXI moisture estimates produced yield simulations that compared favorably with observed yields and with the rainfed model.

The data appear to indicate that the ALEXI model did detect the soil moisture signal from the mixed rainfed/irrigation corn fields and this signal was of sufficient strength to produce adequate simulations of recorded yields over a 10 year period.

Keywords: crop modeling; remote sensing; soil moisture; ALEXI; DSSAT; maximum entropy

1. Introduction

Food security is one of the most pressing issues facing society in the 21st century. Growing populations, competing uses for land and natural resources (e.g., water), and climate change will result in significant stresses on world food supplies. Consequently, methods have been developed to increase yields including the development of new cultivars, more efficient fertilizers, and better irrigation equipment and strategies. Agricultural simulation models are a key component to testing advances in agricultural technology and to predicting crop responses to current and future climate forcings. However, crop biophysical models depend on accurate specification of time-dependent soil moisture conditions to accurately capture impacts of moisture stress on crop condition and at-harvest yield estimates. Typically, soil moisture is estimated using measurements of precipitation (water input) in conjunction with a soil water transport model, which distributes the moisture over the root-zone profile.

Obtaining accurate precipitation inputs to crop and other biophysical models can be challenging, however, particularly in data-limited regions of the world. Precipitation can be measured either by ground-based gauges or through ground-based remote sensing instruments (e.g., radar). However, in many areas the spatial deployment of the measuring equipment and their temporal resolution is not sufficient to drive the simulation models with an acceptable degree of accuracy [1]. For these reasons, there has been substantial interest in the development of satellite remote sensing as a source of precipitation data [2]. Currently, the Tropical Rainfall Measuring Mission (TRMM) satellite is the only operational system in orbit dedicated to precipitation estimation. TRMM employs both radar and microwave sensors to detect and measure rainfall intensity, depths and distribution over an area of the earth between latitudes 50 °N and S along with additional satellites [3]. However, in regions outside the TRMM coverage, there are currently no dedicated operational missions systematically observing precipitation variables.

Some work has been done, and continues to be pursued, in the use of other satellites (particularly polar orbiters) to deduce precipitation. Techniques such as cloud indexing employ the visible and near infrared (IR) bands to classify cloud types and apply pre-assigned rain rates to the classes [4]. Other approaches observe development and evolution of clouds in the visible and near IR channels to deduce precipitation variables from cloud physics [5]. Still other methods employ estimates of cloud temperatures to estimate precipitation [6]. More recent work involves the merging of passive microwave and infrared data to produce composite precipitation products [7]. Algorithms including the Kalman Filter [8] and Artificial Neural Networks [9–11] are employed to assimilate the satellite data. Perhaps the most well-known and mature satellite precipitation products are those associated with the PERSIANN (Precipitation Estimation from Remotely Sensed Information using Artificial Neural Networks) class [7]. These models typically produce precipitation estimates at finer spatial resolution (up to 0.25 °

grid cells) and smaller time steps (6 h or less) than other satellite-based methods. However, according to Gebregioris *et al*. [7], these estimates still contain significant error in their ability to detect rainfall, which makes them problematic for forcing crop biophysical models with the desired accuracy.

On the other hand, a great deal of progress has been made on the estimation of soil moisture from remotely sensed sources. Perhaps the most active area of research has been in the use of microwave instruments. Passive microwave instruments including the European Space Administration's Soil Moisture and Ocean Salinity Mission (SMOS), the Advanced Microwave Scanning Radiometer-Earth Observing System (AMSR-E), and the Defense Meteorological Satellite Program (DMSP) satellites (Special Sensor Microwave/Imager, SSM/I) provide estimates of near-surface soil moisture at temporal frequencies of 1 to 2 days and spatial resolution of around 30 to 50 km. On the other hand, active radars (e.g., Radarsat 1 and 2, ERS-1 and 2, JERS, ENVISAT, ASCAT) can provide surface soil moisture estimates at much finer spatial resolutions (10–100 m) and at similar overpass frequencies. The advantage of radar is that the signal can penetrate clouds and vegetation and is available during nighttime as well as day. The largest negative associated with microwave remote sensing is that it provides estimates of soil moisture only near the surface, usually in the 1–2 cm of the soil column [12]. Future coincident measurements using both passive and active methods will be available from NASA's SMAP (Soil Moisture Active and Passive) instrument due to launch in 2014. Since hydrological or ecosystem models need the water content in the entire root zone, microwave remote sensing alone will not suffice to drive these models. Instead, it is common for microwave data to be assimilated into the models to update surface estimates while the model simulated root zone moisture is retained [13]. In these schemes, root zone soil moisture is not a direct measurement and relies on an accurate specification of error parameters relating the coupling of surface and root-zone soil moisture and precipitation data are still needed to force the land surface model.

However, thermal infrared (TIR) techniques can be used to deduce root zone moisture based on estimates of evapotranspiration (ET) rates from the vegetation canopy. The ratio of actual-to-potential ET is functionally related to available moisture in the soil profile. In remote sensing applications, diagnostic estimates of ET are inverted to infer effective soil moisture availability. TIR ET estimates are related to land surface temperature and vegetation cover fraction estimates from satellite mounted instruments [14]. Among the TIR approaches to ET mapping, the Two-Source Energy Balance (TSEB) model of Norman *et al*. [15] is well suited for estimation of data that can drive hydrologic and biophysical models because it attempts to separate soil evaporation (associated with moisture content in the soil surface layer) from transpiration from the vegetation (related to root-zone moisture). The TSEB has been implemented regionally from field to continental scales using TIR data from geostationary and polar orbiting platforms [14,16]. However, since the TIR signal cannot penetrate clouds, direct retrievals of ET are only available on substantially clear days.

In this study, a continental-scale implementation of the TSEB method known as the Atmosphere-Land Exchange Inverse (ALEXI) model [17] was employed to gain estimates of both surface and root zone soil moisture. The ALEXI soil moisture estimates were then used to drive a standard biophysical crop model (Decision Support System for Agrotechnology Transfer–DSSAT; [18]). The DSSAT source code was modified to read daily soil moisture values in lieu of measured precipitation data and applied to an area in northern Alabama. The yield results from DSSAT driven by the ALEXI soil moisture estimates

were compared to those obtained when the model is driven by ground-based precipitation measurements and to measured yields to benchmark potential performance over data-limited regions.

2. Methods and Materials

The study consisted of the following elements:

(1) Estimation of surface and root zone soil moisture proxy values from ALEXI over the period April 2000 to September 2009. Daily values of either surface or root zone soil moisture were obtained on clear days for which ALEXI simulations were available.
(2) Computation of a vertical soil moisture profile from the ALEXI data consistent with the profile depths required by DSSAT.
(3) Comparison of ALEXI soil moisture values with both rainfed DSSAT values and soil moisture estimates from a simulation using Noah land surface model processed from NASA's Land Information System (LIS) over the same period.
(4) Integration of ALEXI derived soil moisture profiles within the DSSAT model, used in lieu of precipitation data.
(5) Comparison of yield estimates from the ALEXI soil moisture driven model and the DSSAT model driven by the recorded precipitation, and with measured yields.

2.1. Study Site

The primary site for the model comparisons was an area in North Alabama, USA encompassing parts of Limestone and Madison counties. The Tennessee Valley Research and Extension Center in Belle Mina, AL, USA (34°41'22''; 85°53'17") provided the climate data for the study. The Belle Mina Research Center is located in Limestone County and is operated by the Agricultural Extension Service of Auburn University. A meteorological station located at the site collects all relevant climate data including temperature, precipitation, solar radiation, and relative humidity. The experimental station consists of 305 ha of farmland devoted to experimentation on various crop species and agricultural practices. The soils of the area are primarily silty clay loams. Based on data obtained from the web-based county soil survey for North Alabama, the predominant soil is Decatur silty loam—a brownish-red soil with moderate drainage. The soil properties relevant to both ALEXI and DSSAT are given in Table 1. Soil matrix and chemical properties were obtained directly from the survey, while water storage parameters (wilting point and field capacity) were unavailable from the survey so were taken from Clapp and Hornberger [19]. It should be noted that soil parameters taken from parameters developed in crop model due to differing (or vague) definitions of parameters and statistical representations of parameter values (e.g., mean *vs.* median, *etc*.) [20]. This dichotomy could lead to slight inconsistencies between soil moisture representations in ALEXI and DSSAT.

The test site is located in the Southeastern United States, representing a subtropical humid climate. Average annual precipitation of the region is nearly 1,450 mm according to the National Oceanic and Atmospheric Administration (NOAA) Huntsville, Alabama meteorological records. Relatively hot summers and precipitation distributed throughout the year are typical of subtropical humid climates. Although precipitation does occur throughout the year, the Gulf of Mexico region is known to receive

more precipitation during winter months than summer [21]. In fact, the records show that the annual mean precipitation at Belle Mina is 1,453 mm, of which only 297 mm occurs during the growing season (Belle Mina rain gauge record from 2000 to 2009). Consequently, the area includes a substantial percentage of irrigated farm land. About half of the experimental plots are irrigated and the surrounding area contains about 4,000 ha of irrigated land in Limestone and Madison counties that would all fall within the ALEXI footprint of this study.

Table 1. Soil characteristics at Belle Mina, Alabama USA study site.

DSSAT Input Soil Parameters						ALEXI Soil Parameters	
Depth (cm)	**Clay %**	**Silt %**	**Sand %**	**pH**	**Cation Exchange Capacity (cmol/Kg)**	**WP (cm^3/cm^3)**	**FC (cm^3/cm^3)**
0–10	21.0	52.7	26.3	5.3	5.0	0.084	0.360
10–40	34.4	47.8	11.6	5.3	6.2	0.103	0.382
40–100	45.9	29.2	23.3	5.3	5.9	0.138	0.412
100–200	47.5	29.2	23.3	5.3	5.9	0.138	0.412

The DSSAT crop model was run to simulate maize (corn) production in the area. Agricultural production in North Alabama is primarily in corn, cotton and soybean. The surrounding area is similar in climate, soils, and agricultural practices to the study site. There has been a steep increase in corn cultivation in Limestone County between the years 2002 and 2007, from about 2,000 ha to nearly 9,000 ha.

2.2. ALEXI Modeling Framework

2.2.1. Two-Source Energy Balance Model

The ALEXI model was introduced by Anderson, *et al* [17]. The model is an extension of the TSEB approach [15] and treats the land surface as a composite of soil and vegetation components, in contrast to simpler single-source models that treat each pixel as a homogeneous surface. This coupling of the soil and canopy allows the TSEB model to produce an estimate of energy and water fluxes over a wide range of land surfaces from bare soil to partially and complete canopy cover [15,22].

The composite directional radiometric temperature [$T_{RAD}(\theta_L)$] is a function of the fraction of vegetation cover apparent at a sensor viewing angle differentiating the soil and canopy temperature (T_S and T_C) and represented by

$$T_{RAD}(\theta_L) \approx \{f_c(\theta_L)T_c + [1 - f_c(\theta_L)]T_s\} \quad (1)$$

where

$$f_c(\theta_L) = 1 - exp\left(\frac{-0.5\,F}{cos\theta_L}\right) \quad (2)$$

is the fraction of vegetation cover at the thermal sensor viewing angle, θ_L, and F is leaf area index [14,23].

ALEXI computes the soil (subscript ‘s’) and canopy (subscript ‘c’) energy budgets separately, calculating fluxes of net radiation (*RN*), sensible heat (*H*), latent heat (*LE*), and ground heat conduction (*G*) of each component of the soil/canopy system with all energy units in Wm^{-2}:

$$RN = H + LE + G \tag{3}$$

$$RN_s = H_s + LE_s + G \tag{4}$$

$$RN_c = H_c + LE_c \tag{5}$$

Soil and canopy sensible heat fluxes are computed from near-surface temperature gradients and turbulent and diffusive transport resistances:

$$H = H_S + H_C = \rho C_p \left(\frac{T_{ac} - T_a}{R_a}\right) \tag{6}$$

$$H_C = \rho C_p \left(\frac{T_c - T_{ac}}{R_x}\right) \tag{7}$$

$$H_S = \rho C_p \left(\frac{T_s - T_{ac}}{R_s}\right) \tag{8}$$

where ρ is air density, C_p is the heat capacity of air at constant pressure, T_a is the air temperature at a height above the canopy, and T_S and T_C are the soil and canopy temperatures, respectively, T_{ac} is an effective temperature within the canopy (similar to an aerodynamic temperature), R_a is transport resistance between the canopy and the reference height, R_S is the soil surface resistance and R_x is the bulk leaf boundary layer resistance. All resistance terms (sm^{-1}) are discussed in [15], with updates provided by [24–27].

The canopy transpiration term used to compute latent heat (LE_C) is calculated using a modified Priestley-Taylor approximation [28]. The plant transpiration is related to the canopy net radiation divergence RN_C as:

$$LE_C = \alpha_C f_c \left(\frac{\delta}{\delta + \gamma}\right) RN_C, \tag{9}$$

where $\alpha_c$is the Priestley-Taylor coefficient equivalent to 1.3 which can be down-scaled depending on the vegetative stress [17,14,29] and discussed further below, f_c is the fraction of green vegetation, δ is the slope of saturated vapor pressure curve with respect to temperature; and γ is the psychometric constant (0.066 $kPa \cdot ℃^{-1}$). The soil latent heat (LE_S) is computed as the residual of the canopy latent heat and latent heat of the system (LE):

$$LE_S = LE - LE_C, \tag{10}$$

The soil heat flux G is parameterized as time varying (α_g) of the net soil radiation (RN_S):

$$G = \alpha_g RN_S, \tag{11}$$

where α_g is specified using the formulation of Santanello and Friedl [30].

A stressed canopy does not transpire at the estimated potential Priestley-Taylor rate, resulting in overestimation of canopy latent heat. This in turn forces LE_S to become negative in Equation (10). This condition suggests the process of condensation, a situation unlikely during daylight hours. Thus, under canopy stress, LE_C is iteratively reduced from its potential rate until LEs approaches 0 [15].

2.2.2. Regional Implementation

Surface and near-surface temperature measurements usually represent the boundary conditions for traditional TIR-based energy flux models, defined via temperature gradients as in Equation (6). However, measurements of these boundary fields for regional applications are typically acquired with very different sensors (remote sensing and synoptic meteorological stations) and may contain significant and spatially dependent inconsistencies. Biases in the assumed surface-to-air temperature gradient can serve to significantly corrupt surface flux estimates derived from energy balance algorithms [31]. The Atmosphere-Land Exchange Inverse (ALEXI) model was designed for robust regional applications of the TSEB [14,22,32]. An improvement in ALEXI is the incorporation of a time-differencing scheme, representing the time-integrated coupling of the soil-plant-fluxes with the atmospheric boundary layer (ABL) as proposed by Carlson, *et al.* [33] and others. This time-differential implementation serves both to eliminate the need for specification of near-surface air temperature boundary conditions, and makes the model less sensitive to absolute errors in surface temperature retrievals.

The ALEXI model uses a simple ABL closure technique to relate the rise in T_a in the mixed layer to the time-integrated influx of H from the surface [17,34], computing simultaneous energy balances at the surface and in ABL. The TSEB is applied at two times (t_1 and t_2) during the morning hours, approximately at 1.5 and 5.5 h after local sun rise, using radiometric surface temperature estimates derived from geostationary satellites (e.g., Geostationary Operational Environmental Satellite (GOES), *Meteosat*), providing two estimates of instantaneous H flux estimates H_1 and H_2. Time changes in surface temperature are known to be correlated with the LE and H fluxes: a wetter land surface warms slowly as compared to the dryer surface, thus requiring more energy for evaporation [35]. ALEXI assumes a rise in H through a linear functional form for $H(t)$. The time integrated heat flux is then:

$$\int_{t_1}^{t_2} H(t)dt = \frac{1}{2}[H_2 t_2 - H_1 t_1], \tag{12}$$

The energy conservation relationship between the rise in boundary layer height (z) and potential temperature of the mixed layer (θ_m) to the time-integrated H from the surface is given as [36]:

$$\int_{t_1}^{t_2} H(t)dt = \rho C_p(z_2\theta_{m2} - z_1\theta_{m1}) - \rho C_p \int_{z_1}^{z_2} \theta_s(z)dz, \tag{13}$$

where $\theta_S(z)$ is the early morning potential temperature profile (near time = t_1). At the surface, the mixed layer potential temperature is related to the air temperature by

$$\theta_m = T_a\left(\frac{100}{p}\right)^{R/C_p}, \tag{14}$$

where p is the atmospheric pressure, and (R/C_p) is parameterized as 0.286 [14].

2.2.3. ALEXI Input Datasets

The ALEXI model has been applied over the continental United States (CONUS) from April 2000 to the present day [14]. The model is run daily at 10 km spatial resolution. Input data sources used in the ALEXI model execution over CONUS are described below.

(i) Surface radiometric temperature and solar insolation data

Surface radiometric temperature (T_{RAD}) data over CONUS used in the ALEXI runs described here were generated using the GOES–East/West sounder instruments. The GOES sounder at channel 4 (10.7 μm) has a spatial resolution of ~10 km and thermal radiances were regridded to the ALEXI grid [14,37]. Atmospheric and emissivity corrections used to retrieve surface radiometric temperature are described in [14].

Incoming solar and long wave radiation is estimated at 10 km spatial resolution using GOES [38]. These radiation components are required for the computation of *RN* at the land surface (soil + canopy) using diagnosed values of T_S and T_C and parameterized values of surface albedo and emissivity.

(ii) Surface and upper air meteorological data

Surface and upper air meteorological inputs to ALEXI, such as mean wind speed near the land surface, vapor pressure and surface pressure, are currently obtained from the National Center for Atmospheric Research Weather Research and Forecasting (WRF) model [39]. The NCAR WRF simulations were run at a 40 km spatial resolution and spatially interpolated to the ALEXI grid.

Atmospheric lapse rate profiles used for the ALEXI ABL growth model were also obtained from the 3-dimensional WRF simulations. Temperature and mixing ratio atmospheric profiles are also used for the atmospheric correction of GOES brightness temperatures.

(iii) Land surface and canopy data

The vegetation cover fraction and Leaf Area Index (LAI) variables required for ALEXI are obtained from standard Moderate Resolution Imaging Spectroradiometer (MODIS) LAI 8-day product at 1 km spatial resolution. The 1 km MODIS LAI product is mosaicked and re-projected to the ALEXI grid with the MODIS Reprojection Tool [14]. Land cover classification is obtained from the University of Maryland (UMD) 1 km global land cover product [40]. The 1 km resolution of the UMD dataset is made consistent with ALEXI by using computing the percentage of each land cover type sampled from the 1 km dataset for each 10 km ALEXI grid cell.

2.3. Available Water Derived from ALEXI

The TSEB component of ALEXI partitions the total system *LE* flux into soil evaporation (LE_s) and canopy transpiration (LE_c) sub-components. These fluxes in turn are largely controlled by soil moisture in the surface layer and the root-zone layer, respectively, and by energy available to each component. In general, wet soil moisture conditions lead to increased *LE* (decreased *H*) and a depressed morning surface temperature amplitude, while dry soil moisture conditions lead to decreased *LE* (increased *H*) and an increased morning surface temperature amplitude. Anderson *et al*. [14] and Hain *et al*. [37,41] outline a technique for simulating the effects of soil moisture on *LE* estimates from ALEXI using a soil moisture stress function, relating the value of the fraction of actual to potential evapotranspiration (f_{PET}):

$$f_{PET} = \frac{LE}{PET}, \tag{15}$$

to the fraction of available water (f_{AW}) in the soil profile:

$$f_{AW} = \frac{\theta_{ALEXI} - \theta_{wp}}{\theta_{fc} - \theta_{wp}}, \quad (16)$$

where θ_{fc} and θ_{wp} are the volumetric soil moisture contents at field capacity and permanent wilting point, respectively (Table 1). Normalization by PET reduces sensitivity to available energy, better isolating variations in evaporative flux due to soil moisture [16]. In many prognostic modeling frameworks, a semi-empirical linear or non-linear relationship is defined between f_{PET} and f_{AW} to account for effects of soil moisture depletion on the surface evaporative fluxes [14,37,41]. Assuming a linear relationship,

$$\theta_{ALEXI} = \left(\theta_{fc} - \theta_{wp}\right) * f_{PET} + \theta_{wp} \quad (17)$$

Retrieval of SM from diagnosed evaporative fluxes (the inverse of the prognostic approach) should be reasonable when soil moisture is between field capacity and the permanent wilting point, but will lose sensitivity as soil moisture exceeds θ_{fc} and approaches saturation. While Equation (17) requires specification of soil texture-specific values of θ_{fc} and θ_{wp}, these local constants fall out in the computation of standardized temporal anomalies. Standardized anomalies in θ_{ALEXI} can be therefore computed directly from f_{PET} without requiring soil texture information. It is assumed that the relative contributions to ET from the surface and root-zone SM are related to the observed vegetation cover fraction as viewed from nadir (f_c). Over sparsely vegetated surfaces ($0 \leq f_c \leq 0.3$), ALEXI *LE* is dominated by direct soil evaporation and reflects soil moisture conditions in only the first 1-2 centimeters of the profile, similar to an effective sensing depth of microwave sensors [42]. However, over dense to full vegetation cover ($f_c > 75\%$) and under well-watered conditions, ALEXI *LE* is predominantly partitioned to canopy transpiration, and soil evaporation becomes negligible in comparison. In this case, f_{PET} is governed by moisture conditions in the plant root zone. Between these two extremes (sparse to full vegetation cover), ALEXI provides a composite of both surface and root-zone soil moisture information, with relative influence related to f_c. Therefore, θ_{ALEXI} values represent a composite of surface and root-zone soil moisture conditions depending on surface vegetation conditions, which can be expressed conceptually as:

$$\theta_{ALEXI} = [1 - f_c]\theta_{ALEXI_{sfc}} + f_c\theta_{ALEXI_{rz}}, \quad (18)$$

In this study, $\theta_{ALEXI_{sfc}}$ and $\theta_{ALEXI_{rz}}$ are not retrieved independently; however, Equation (6) provides a conceptual framework for comparison with microwave and land surface model (LSM) soil moisture estimates. In a previous study, Hain, *et al*. [41] evaluated ALEXI f_{AW} retrievals in comparison with ground-based soil moisture observations over a multi-year period (2002–2004) from the Oklahoma Mesonet and found reasonable temporal and spatial agreement (RMSE values around 20% of mean observed soil moisture).

2.4. Agricultural Simulation Model

The Decision Support System for Agrotechnology Transfer (DSSAT; [18]) crop modeling system is the de-facto standard in crop modeling across the world. In addition to predicting crop yield, DSSAT can also be used to assess water demand for supplemental irrigation and associated nutrient uptake. DSSAT is a framework for biophysical modeling and includes a suite of more than 25 different crop

models [43,44]. The framework allows users to initialize the model with appropriate soil properties and genetic information to describe the local crop and cultivar characteristics. It uses daily meteorological data and local crop management practices in order to conduct the simulations at daily or shorter time steps. The state variables in the soil include soil moisture, and nitrogen and carbon content in each individual soil layer or horizon [18]. DSSAT integrates the soil, crop phenotype, weather and management options to simulate crop growth and development and to predict crop yield. The crop models require daily minimum and maximum air temperatures, precipitation and solar insolation, in addition to the crop management data (such as planting date, seed cultivar, soil type, nutrient loading). The output is end-of-season crop yield as well as nutrient, soil moisture and plant stress variables [18]. The crop simulation models used in DSSAT have been evaluated extensively across the world as well as in the Southern USA [18,45–47].

Since DSSAT crop models use daily weather data as input, this allows for using current weather conditions for evaluation of the models with experimental data. However, it also allows for scenario testing using long-term historical and future data for scenario evaluation. This can include climate variability as well as climate change using future climate change scenarios. The DSSAT system has been employed to help with development of water management plans for the agricultural sector in Georgia [48] and is currently the basis for a real-time crop stress evaluation to monitor drought conditions in the Southeastern United States [49,50].

Although DSSAT was originally developed as a field scale model, it has been employed in regional analysis before. For example, McNider, *et al*. [49] describe the GridDSAT model which operates at an approximately 5 km grid scale to simulate plant stress in the Southeastern US and contributes to the United States National Drought Monitor. Earlier, Heinemann, *et al*. [51] employed DSSAT with a GIS to forecast regional irrigation water demands in Brazil. Fang, *et al.* [52,53] have integrated spatially distributed MODIS vegetation indices with DSSAT for corn yield estimation in the mid-western US, while Gijsman, *et al*. [54] describe the use of the coarse-scale World Inventory of Soil Emission Potentials (WISE) soils database in DSSAT. Finally, White, *et al*. [55] summarize studies that have used crop models, including DSSAT, to predict the effects of climate change on regional crop yields throughout the world. Typically, as done here, these previous studies involve the use of regionally representative soils and climate information into DSSAT in order to produce yield forecasts that represent the regional response. The difference here is that we are driving the model with a spatially integrated soil moisture signal in lieu of a spatially integrated rainfall product such as NEXRAD or NWS Stage IV precipitation.

Of particular interest in the context of this study is the soil moisture mechanics of DSSAT. Moisture storage and infiltration within the soil column are based on a simple vertical storage routing concept. DSSAT is a field scale model, and does not consider lateral movement of water. Water is stored in a particular layer until the drained upper limit (DUL) of that layer is met, at which point drainage into the next layer below occurs. Plant uptake of moisture is allowed until the soil wilting point is approached. Potential ET can be computed using either the Priestley-Taylor approximation [27] or the full Penman-Monteith combination method [56] depending on the availability of data. Soil limited evaporation is then computed using a diffusivity approach with an empirical transfer coefficient [57].

2.5. Development of Soil Moisture Profiles from ALEXI AW

Since ALEXI retrievals can be interpreted as either surface water content or total root zone estimates depending on current vegetation cover fraction [36], it is necessary to compute a vertical soil moisture profile to correspond to the profile in DSSAT. Approaches to estimating SM profiles have been discussed by several authors (e.g., [58,59]). These include regression, inversion, knowledge-based, and combination methods. A combination method that employs remotely sensed observations from ALEXI together with a water balance operation has been used here since it makes maximum use of the remotely sensed data.

An entropy-based approach to soil moisture profile development was presented by Al-Hamdan and Cruise [59] and extended by Singh [60], and then further evaluated by Singh [61]. Application of the technique requires a surface moisture estimate and an estimate of total root zone water content, one of which can be inferred from ALEXI f_{PET} estimates. The method is based on the principle of maximum entropy (POME) expounded by Jaynes [62,63]. The principle states that if inferences are to be made from incomplete data, they should be based on the probability distribution that possesses maximum entropy permitted by the prior information [59]. Using an approach originally employed by Chiu [64] to compute vertical velocity distributions in open channels, Al-Hamdan and Cruise [59] assumed a uniform distribution of soil moisture through the soil column to develop a set of profiles corresponding to all possible cases. In the situation considered here, only two cases are required—the case of a wet surface layer with drier soil underneath, and the reverse case, e.g., a dry surface with wetter conditions underneath. The application of POME to develop a one-dimensional soil moisture profile requires two constraints: the total probability constraint:

$$\int_{\Theta_L}^{\Theta_0} f(\Theta)d\Theta = 1, \tag{19}$$

and the constraint to satisfy mass balance:

$$\int_{\Theta_L}^{\Theta_0} \Theta f(\Theta)d\Theta = \overline{\Theta}, \tag{20}$$

where Θ = effective saturation= $\frac{\theta - \theta_r}{\eta - \theta_r}$ and $\overline{\Theta}$ is the mean value of the soil column, η = soil porosity and θ_r is the irreducible water content of the soil; whereas Θ_0 and Θ_L are the surface and bottom effective saturations. The second constraint serves to connect the first moment in probability space to the mean water content of the soil column in physical space. The Shannon entropy is given by [65]:

$$I = -\int_0^{\infty} f(x)\ln\big(f(x)\big)\,dx, \tag{21}$$

where $f(x)$ is the probability density function (pdf) of the variable. Maximizing I in Equation (21) for the uniform pdf subject to the constraints above, Chiu [64] developed the 1-D profile of a variable decreasing monotonically from the surface down using the method of Lagrange multipliers (put into soil moisture terms by Al-Hamdan and Cruise [59]):

$$\Theta(z) = \frac{\ln\left[\exp(\lambda_2\Theta_0) - \lambda_2 \exp(1-\lambda_1)\left(\frac{Z}{L}\right)\right]}{\lambda_2}, \quad (22)$$

The Lagrange multipliers (λ's) can be solved from application of the constraints and boundary conditions (surface effective saturation, Θ_0 and mean effective saturation value of the soil column $\overline{\Theta}$), z is calculation depth, and L is total depth of the column.

Following the same procedure, Al-Hamdan and Cruise [59] developed the profile for the second case (monotonically increasing vertically):

$$\Theta(z) = \frac{\ln\left[\exp(\lambda_2\Theta_0) + \lambda_2\exp(1-\lambda_1)\frac{z}{L}\right]}{\lambda_2}, \quad (23)$$

Relationships between the Lagrange multipliers and the constraints and boundary conditions have also been developed, as in the first case, with the resulting system of nonlinear equations solved for the multipliers by a technique given by Barbe *et al*. [66].

3. Integration of ALEXI SM within DSSAT

3.1. Gap-Filling ALEXI SM Time Series

Since the purpose of the study was to drive the crop simulation model with ALEXI observations, only values during the growing season (planting to harvest) for each year were utilized. There are roughly 165 days in the growing season in north Alabama resulting in a total of approximately 1,650 days in the growing season over the period of record (2000–2009). The standard ALEXI spatial resolution is 10 km so the location of the climate station at Belle Mina fell within a single ALEXI pixel. Over the study period, clear-sky ALEXI retrievals were available in that pixel for 513 days (31.1% of total). Correlation analyses revealed a generally strong spatial correlation between the target pixel and adjacent pixels within a 3 × 3 sub-grid (r > 0.8) so that a regional approach to the ALEXI data retrievals appeared reasonable. This is likely due to the fact that the surrounding area is very homogenous in terms of soil type, land cover, climate, and irrigation conditions. Therefore, the time-series of ALEXI-based f_{AW} was gap-filled using data from pixels within this 3 × 3 grid increasing temporal coverage to 678 days (41%). Of this total, 591 values were recovered from either the target pixel or one of the three pixels immediately adjacent to it so that ultimately about 87% the ALEXI retrievals utilized came from the pixel containing the Belle Mina station or one of the three adjacent pixels. More importantly, 75.6% of the retrievals utilized came from the Belle Mina pixel itself. A consequence of note relevant to the expansion of the ALEXI footprint (however modest) would be that moisture conditions in the adjacent irrigated land in Limestone and Madison Counties would be included in the ALEXI signal.

3.2. Intercomparison of Soil Moisture Time Series

To evaluate the reasonability of the ALEXI-derived soil moisture dynamics within the study region, ALEXI soil moisture time series were compared with SM simulations from a prognostic LSM forced with non-local precipitation data. Simulations of daily SM at several depths were generated with the

Noah LSM (v 2.7.1; [67]) run within the NASA LIS at 10 km resolution. The LIS, developed at NASA Goddard Space Flight Center, is a software framework to integrate both satellite and ground-based observations into advanced LSMs [68,69]. The Noah LSM is a one-dimensional land-vegetation-atmosphere transfer (SVAT) model that requires three input types: initial conditions of the soil and states; boundary conditions, upper boundary (atmospheric) fluxes or states and the lower (soil) fluxes and states; and parameters which are the functions of soil, vegetation, topography and various other land surface characteristics [67]. Noah solves the governing equations of the SVAT based on the inputs to predict the surface fluxes as well as the soil states.

Noah outputs soil moisture estimates associated with 4 soil layers: 0–10 cm; 10–40 cm; 40–100 cm; and 100–200 cm. For this experiment, Noah soil moisture data were available at a daily time step for the period of 2000–2007 at 10 km spatial resolution. Daily time-series were extracted at the grid cell containing the Belle Mina site and total soil water to a depth of 200 cm was determined by a depth-weighted averaging of the four Noah SM layers. Since ALEXI data are not available daily over the study area, both ALEXI and Noah time-series were used to compute 14-day averages to facilitate intercomparison. Furthermore, to focus comparison on the models' ability to simulate short–term soil moisture dynamics, the longer term variation (annual cycles) were removed from each time-series through computation of normalized anomalies ($x_i - \bar{x}$)/σ. Where x_i is composite soil moisture estimates whereas $\bar{x}\ and\ \sigma$ are the multi-year 29 days centered (−14:+14 days) mean and standard deviation, respectively.

In a similar fashion, the ALEXI soil moisture series was compared to the DSSAT soil moisture anomalies, generated by a DSSAT simulation driven by the actual precipitation recorded at the site. This was done in order to ensure that the ALEXI soil moisture climatology was reasonably representative of the DSSAT soil moisture dynamics.

3.3. Updating DSSAT with ALEXI Soil Moisture

The final step in the analysis involved comparison of soil moisture and yields generated with DSSAT when forced with observed rainfall (standard mode) and with ALEXI-derived soil moisture profiles. For the ALEXI-driven simulations, soil moisture profiles within the DSSAT framework were periodically updated based on a set of rules devised to minimize impacts of noise in the remotely sensed dataset. A filtering system was devised such that the DSSAT soil moisture dynamics would be allowed to proceed normally to the extent possible so that updating with ALEXI/entropy profiles would be done only when necessary. This rule was promulgated under the assumption that, since it incorporates the soil physics, DSSAT soil moisture dynamics would be more accurate in the short run than noisy remote sensing estimates. For example, during periods when successive days of ALEXI retrievals were available, only the first day's estimate would be employed so that DSSAT could function normally during following days until a gap in the ALEXI data was encountered. This is justifiable because root-zone and total layer soil moisture are a slow varying quantity (*i.e.*, on the orders of days to weeks) and successive updates using ALEXI may introduce significant day-to-day noise in the DSSAT SM profile. Then, the next ALEXI value after the gap would be employed to update DSSAT, and so on. On average, updates were accomplished about every 10–12 days following this system.

First, the ALEXI f_{PET} data were separated into surface values and root zone values according to the observed MODIS fraction of vegetation cover as previously discussed: $f_c \leq 0.4$ surface; $f_c \geq 0.75$ root zone; $0.4 \leq f_c \leq 0.75$ combination of surface and root zone. For purposes of this analysis, values where $0.4 \leq f_c \leq 0.75$ were also utilized to get the total water available in the soil column in order to compute the mean effective soil moisture.

In performing the data separation described above, it quickly became evident the retrievals associated with surface moisture would be sparse or non-existent during the growing season. As the crop grows, the vegetation cover fraction naturally becomes greater until the surface is largely obscured by vegetation. Thus, virtually all retrievals during the growing season are interpreted as either combination or root zone values and are suitable for determination of total moisture content.

On the other hand, no values were assigned to the surface, so the surface boundary conditions for the POME profile calculations were unavailable. Since the surface values were unavailable, an assumption that is common in hydrology was employed: initial conditions were assumed based on antecedent precipitation [70,71]. If soil moisture increased in the days after clear-sky ALEXI retrieval, it was assumed that rainfall must have occurred at some point during this period. Therefore, it was deduced that the surface would have been wet to some extent. In these cases, the common, assumption is one of mean or median saturation conditions [70,71]). Here we assume mean (50%) saturation. Conversely, if total soil moisture had decreased in the interval, then it was assumed that no precipitation occurred and the surface was assumed to be at wilting point. Although it has been shown by Al-Hamdan, *et al*. [59] that the entropy profile must converge to the true profile if the mean and boundary conditions are correctly specified, incorrect specifications of these values introduce errors into the analysis. The shape of the soil moisture profile can impact the water uptake of the plants depending on their root distribution. Comparisons to observed yields can serve to quantify this error to some degree.

The ALEXI retrievals also required further filtering to remove spurious readings that occur when slight cloud cover interferes with estimation of the change in land surface temperature thus leading to incorrect calculation of sensible heat loss. The filter removes highly variable f_{PET} readings associated with cover fractions greater than 0.4 since it is unlikely that root zone soil moisture would demonstrate such rapid fluctuations.

Using the procedure described above, the DSSAT profile was updated 97 times over the study period for an average of 9.7 times per year. The rest of the time, DSSAT was allowed to proceed normally.

4. Results and Discussion

As discussed above, the ALEXI soil moisture retrievals contain errors and the profile development and assumptions inherent in the entropy method may add to those errors. For this reason it is important to compare the results to standard and well accepted alternative products. The GSFC LIS discussed in Section 3.2 is one of those alternatives. Comparisons of ALEXI f_{PET} anomalies with Noah SM anomalies are shown in Figure 1, while the similar comparison of ALEXI to DSSAT is shown in Figure 2. These figures demonstrate that ALEXI does appear to offer a fair representation of the high frequency soil moisture fluctuations for the study area despite the ~10 day update frequency, and that it correlates well with the soil moisture dynamics in the rainfed DSSAT model. In fact, the correlation is slightly better with DSSAT as compared to LIS (r = 0.74 *vs.* 0.58). In this regard, even though the ALEXI retrieved

signal is undoubtedly sensing both rainfed and irrigated farmland, the anomalies should be comparable since they are being standardized by the mean in each case.

Based on these results it seems reasonable to assume that ALEXI estimated soil moisture would offer a reasonable approximation to a rainfed DSSAT moisture regime and promises to produce realistic yields. However, since the ALEXI footprint is covering a mixed rainfed-irrigated environment, it is also important to compare to irrigated yield results. For this reason, DSSAT was also run with the supplemental irrigation option enabled such that irrigation would occur when modeled soil moisture was below 50% of field capacity. The results of the yield comparison between the rainfed and irrigated DSSAT model and the ALEXI forced model are shown in Figure 3. Table 2 gives the annual yields and other pertinent information on the simulations.

Figure 1. (**a**) Anomaly time series plot between LIS (yellow) and ALEXI (blue) 14-day soil moisture composite at Belle Mina, Alabama for the period of 2000–2010; (**b**) Scatter plot of the anomalies between LIS and ALEXI again at the Belle Mina, Alabama.

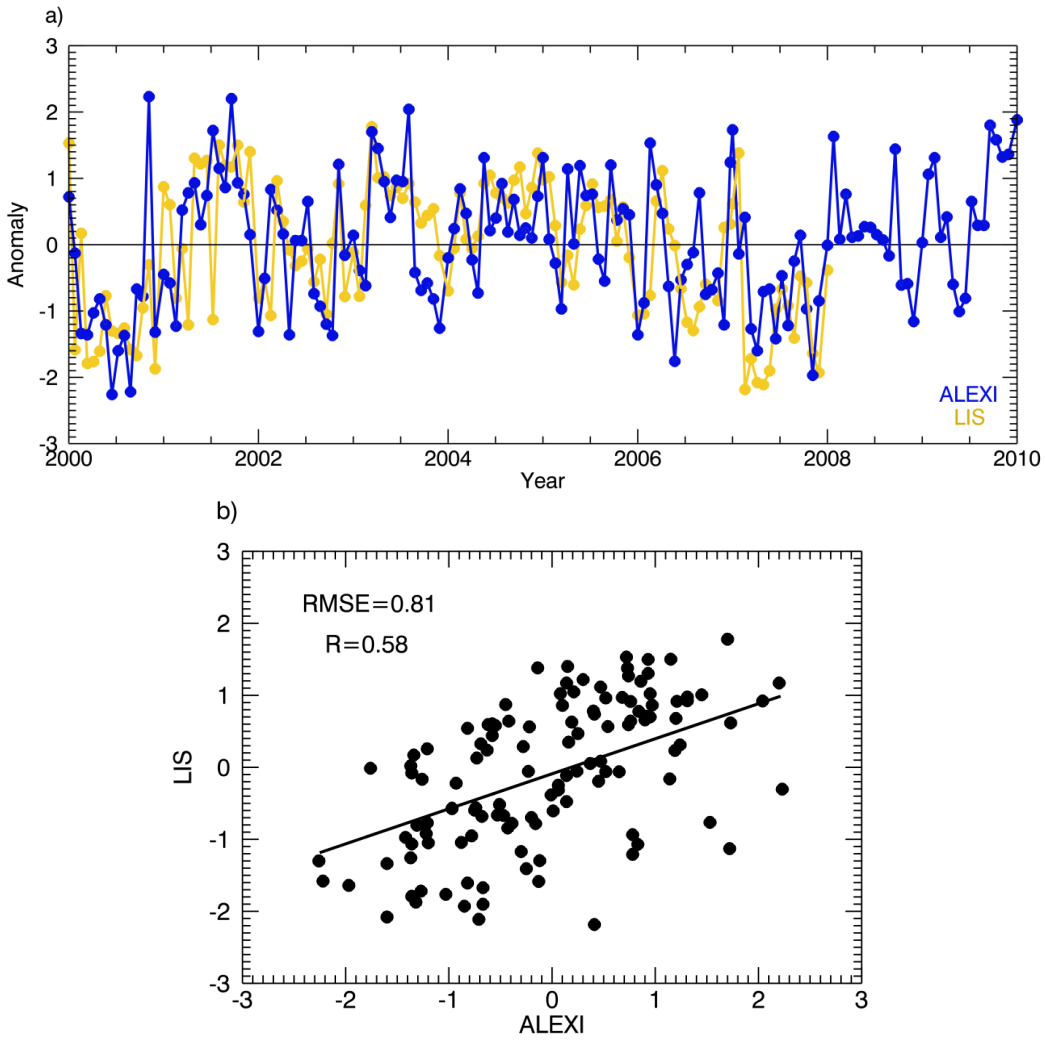

Figure 2. (**a**) Anomaly time series between DSSAT rainfed (green) and ALEXI (blue) 14-day soil moisture composite at Belle Mina, Alabama for the period of 2000–2010; (**b**) Scatter plot of the anomalies between DSSAT and ALEXI again at the Belle Mina, Alabama.

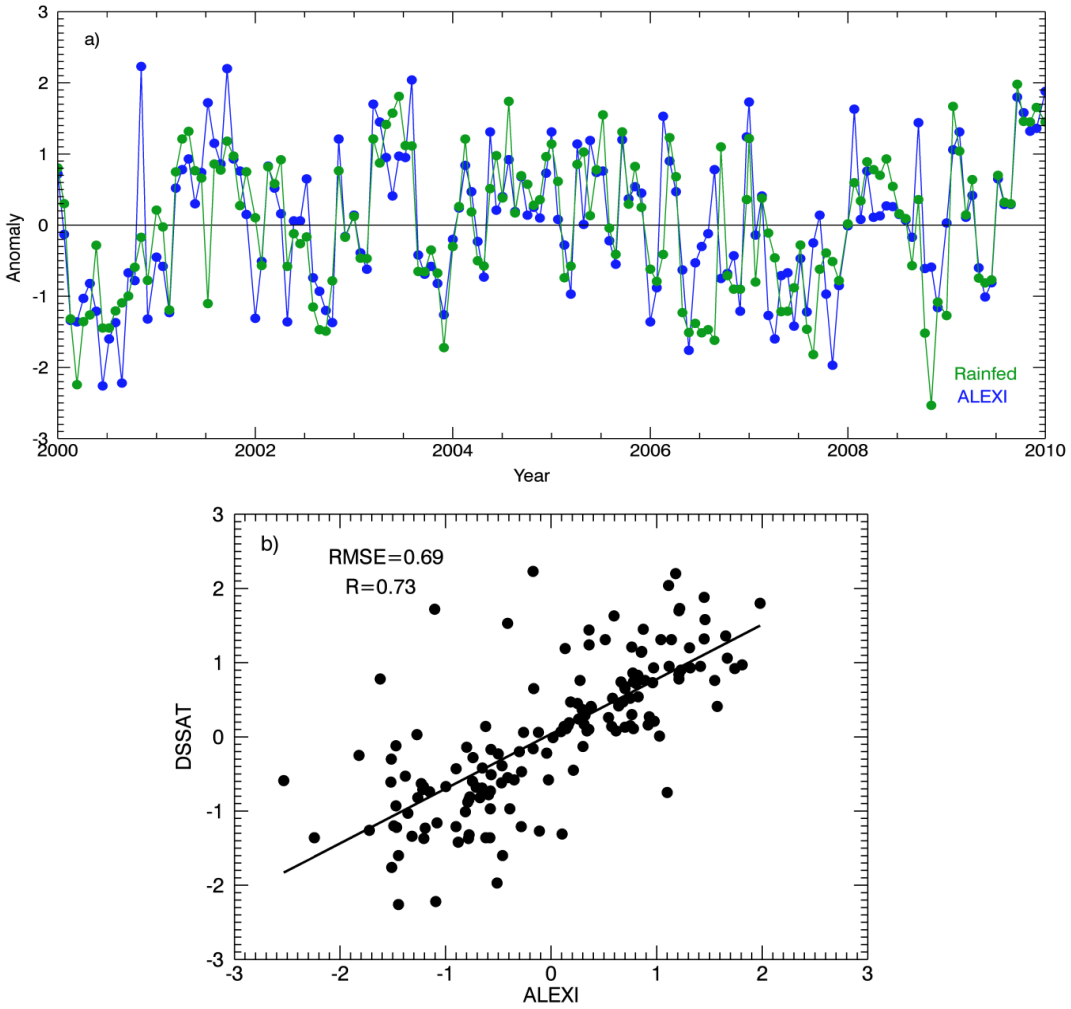

Figure 3. Comparisons of DSSAT rainfed (green), irrigated (red) and ALEXI-driven (blue) crop yields

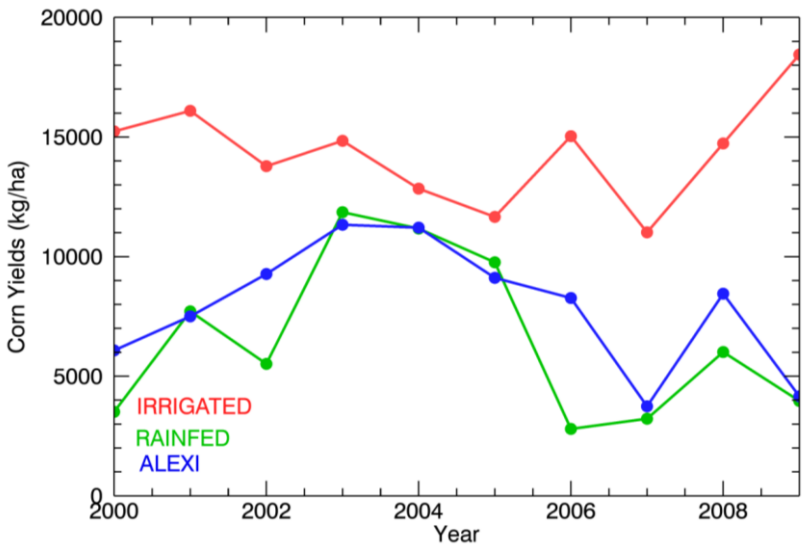

Table 2. DSSAT yield comparisons with pertinent data.

Year	Planting Day	Rainfed Yields (kg/ha)	Irrigated Yields (kg/ha)	ALEXI Yields (kg/ha)	Number of Updates
2000	07-Mar	3,512	15,234	6,078	7
2001	27-Apr	7,711	16,095	7,501	8
2002	17-Apr	5,516	13,781	9,272	8
2003	30-Apr	11,856	14,844	11,332	11
2004	23-Mar	11,173	12,839	11,211	11
2005	20-Apr	9,761	11,661	9,112	10
2006	17-Apr	2,797	15,033	8,269	12
2007	04-May	3,223	11,013	3,741	9
2008	24-Apr	6,011	14,729	8,449	12
2009	23-Mar	3,967	18,443	4,159	9
	Mean	6,552.7	14,367.2	7,912.4	

In interpreting these results, it must be remembered that the rainfed model is driven by precipitation recorded at a single point, while the ALEXI model is forced by a spatially integrated LST product. For this reason, comparisons are used primarily in a qualitative manner to judge the realism of the ALEXI results in comparison with DSSAT run in standard (point) mode and under fully irrigated conditions. Thus, the natural (rainfed) and irrigated yields serve as effective benchmarks for the ALEXI-forced yields. That said, the results indicate that yields from the DSSAT model forced by ALEXI soil moisture profiles generally simulated the overall temporal pattern of the rainfed results, as indicated by a correlation of 0.79, and in many years matched those yields extremely well. Further, a two-sample *t*-test of the mean values under the assumption of equal variances yielded a *p* value of 0.33, indicating that the null hypothesis of equal means cannot be rejected. As could be expected, the ALEXI-forced yields generally fell between the rainfed and irrigated yields and that the increase above DSSAT rainfed yields is most notable during the drought years while the three models were in fair agreement for the wetter years in the record (2003–2005). Following up on this point, the figure reveals that the largest discrepancies between the rainfed and ALEXI forced DSSAT yields in terms of percent absolute differences were observed in 2000, 2002, 2006 and 2008 where DSSAT-ALEXI yield estimates were larger than DSSAT-rainfed by 40–196%. It should be noted that these years encompass some of the most significant drought years in recent history in the Southeastern US. The sampling of adjacent irrigated fields within the ALEXI pixel is likely a significant source of discrepancy in the yield estimates between the DSSAT-ALEXI and DSSAT-rainfed simulations and thus the yields were nudged more toward the irrigated values. In addition, since the rainfed DSSAT model was forced with point precipitation recorded at the Belle Mina gauge, it may have missed rainfall that occurred at nearby locations within the ALEXI footprint.

The issue can be further explored through a comparison of total soil moisture developed by the rainfed and ALEXI forced models. Seasonal average soil moisture estimated by the two models are compared in Figure 4, and tabulated with percent differences in Table 3. The mean annual percent difference in soil moisture between the ALEXI and rainfed DSSAT models was 6.12% per growing season. However, in terms of soil moisture, the positive discrepancies in 2006 and 2008 of 6.7% and 9.6% respectively would not seem to be the sole cause of the yield differences of 195.6% (2006) and

40.56% (2008). Clearly, other factors are at work in the transition of soil moisture availability to yield in the model and further analysis of this issue can lead to insights related to the ability of DSSAT to simulate crop growth in drought years.

Figure 4. Comparison of total soil moisture (mm) between ALEXI and rainfed DSSAT.

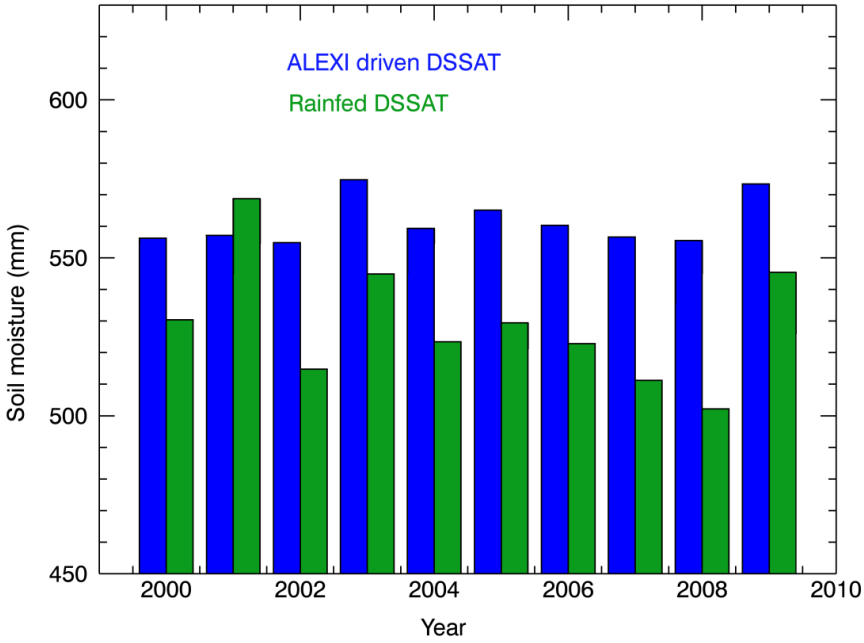

Table 3. Seasonal total soil moisture comparison.

Year	Rainfed S.M. (mm)	ALEXI S.M. (mm)	% Diff
2000	530.40	556.16	4.64
2001	568.70	557.18	−2.08
2002	514.81	554.82	7.21
2003	544.94	574.74	5.19
2004	523.43	559.30	6.42
2005	529.51	565.12	6.32
2006	522.86	560.30	6.69
2007	511.29	556.67	8.15
2008	502.21	555.55	9.95
2009	545.46	573.43	4.88

The situation can be illuminated by examination of the soil moisture dynamics during 2006, as shown in Figure 5. First, the figure confirms that 2006 was a drought year in northern Alabama as the soil moisture in the rainfed model evidenced a continuous steep decline throughout the growing season. On the other hand, the ALEXI updates evidenced by the sharp spikes in the soil moisture in the ALEXI driven model tend to maintain consistently higher soil moisture content throughout. The three profile plots on the bottom half of the figure correspond to the profile comparisons at the first three update points (starting on 7 June) evidenced in the plot. As shown, the shape of the ALEXI profiles generally correlates with the rainfed plots, but shows a slight positive bias indicative of a larger mean moisture value. As shown in the plot, this bias is generally on the order of 50 mm or less distributed throughout a

depth of 200 cm. The significant dates in the crop phenology for 2006 are marked on the plot so that it is obvious that the positive bias occurs during the later part of the silking and throughout the grain filling stages of the corn growth cycle. This greater soil moisture worked to decrease the plant stress during this critical growth phase and thus resulted in larger yields compared to the rainfed, drought stricken model.

Figure 5. Comparison of DSSAT Rainfed and ALEXI forced soil moisture dynamics for the year 2006.

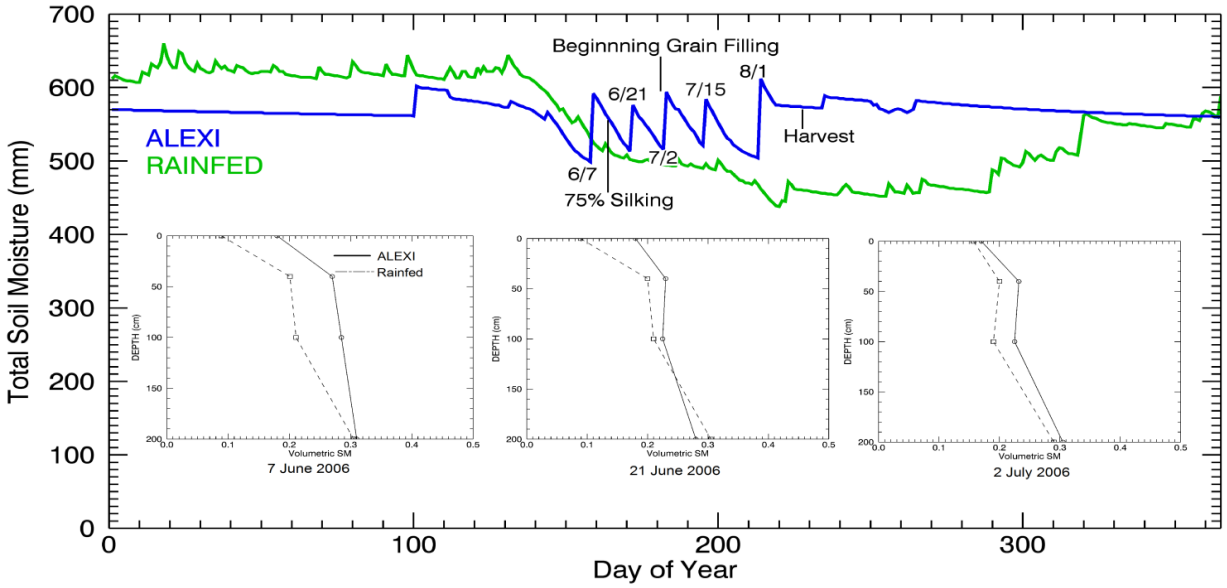

Analysis of Figure 5 indicates that the soil moisture updates raised the moisture to a fairly even level each time throughout the silking and grain filling stages. Therefore, it does appear that the signal that was detected by the ALEXI model may be indicative of an irrigation scenario in which a fairly constant moisture rate is applied to the crop.

Further evaluation of the ALEXI forced yields is provided through a comparison with the annual county yields as given by the US Agriculture Department annual census data. The reported average yields of Limestone and Madison counties were averaged for this comparison since the ALEXI retrievals actually came from both counties. Yields from the irrigated and ALEXI-forced models are compared to reported NASS yields in Figure 6. Dryland yields are not shown since the point-driven DSSAT yields would not be expected to compare with county wide observations for even one county, much less two. However, the NASS yields include both irrigated and dry land production and it should be noted that the approximately 4000 ha of irrigated land in the area still represents only about 29% of total crop land within the two counties.

Thus, the reported yields will not approach the yields associated with full irrigation except during the wetter years. The results indicate that both the ALEXI-forced and irrigated model yields were closer to the reported values during wetter years of 2003–2005 and further apart during the drought years. Even so, the figure shows that the ALEXI-forced model was a fair representation of the NASS yields for several years and closer than the irrigated yields in nearly all cases. In fact, the Root-Mean-square Error in the ALEXI model yield estimates was 35.2 bu/ac which represents only 28% of the mean value. Overall, the ALEXI yields did show a positive bias of 4.7% compared to the NASS yields indicating that

the ALEXI signal perhaps detected more water than was available on a county wide basis in the area. In addition, the DSSAT model was not calibrated to county wide yields in advance so it too contains errors, which would have contributed to the overall errors in the results.

Figure 6. Irrigated and ALEXI forced DSSAT Yields compared to NASS County Yields for Limestone and Madison Counties, AL

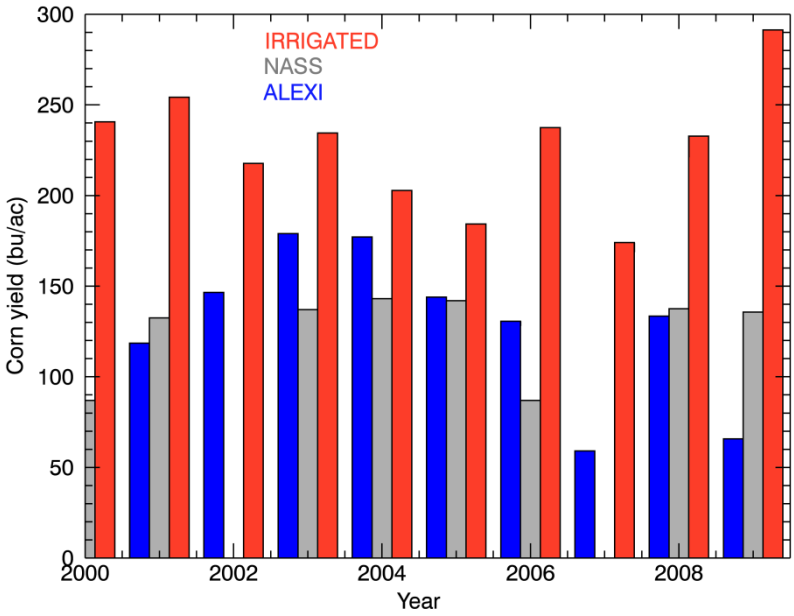

5. Errors and Uncertainties in the Study

Aside from errors inherent in DSSAT itself, which are discussed in the cited references, there are several sources of error associated with the overall approach followed in the study. These uncertainties include those introduced by the regionalization of the DSSAT model, errors inherent in the ALEXI model, and errors associated with the entropy method chosen to estimate vertical profiles from the ALEXI derived root zone soil moisture values.

The DSSAT model was formulated in a manner to represent the crop response for the area incorporated within the ALEXI footprint. This entailed selections of a soil profile and an agricultural management plan for the area. The soil survey revealed that the soils within the footprint were nearly all classified as silty loams (69.3%) or silty clay loams (28.9%). Since silty loam soils predominated, the profile for Decatur silty loam soils was used in the model. While this selection introduces some error into the analysis, sensitivity runs on the soil parameters resulted in an average 2.8% difference in yields associated with the soil matrix.

Similarly, the ALEXI footprint incorporated multiple farms operating under individual management plans and producing more than one crop. In this study, the DSSAT model was executed in the optimization mode so that nutrient applications were done in a manner to maximize yields. Furthermore, a survey of the NASS Cropscape Database (http://nassgeodata.gmu.edu/CropScape/) revealed that corn is the dominant crop in the region covering approximately 20% of the area. Other crops appearing at lesser acreages in the footprint include cotton and soybeans. However, it is known that corn is the most water intensive of the crops and receives the overwhelming majority of the irrigation (70), so the corn

acreages could be expected to dominate the ALEXI soil moisture signal. The strong correlation (r = 0.71) of the ALEXI soil moisture anomalies with the natural rain fed corn soil moisture regime affords confirmation that the corn soil moisture signal in conjunction with the silty loam soils does dominate the footprint. The correlation (r = 0.58) of ALEXI and LIS anomalies indicates that the ALEXI detected soil moisture signal is realistic for the area.

The Maximum Entropy Method that was employed to produce the vertical soil moisture profiles input to the DSSAT model also contains unavoidable errors. In this study, profiles were produced from ALEXI data at an interval of 10–12 days that may or may not have encompassed a rain event. In the comparable case described by Al-Hamdan and Cruise [59] and further evaluated by Singh [60,61], the average error in the profiles, compared to known data, was 2.1%. However, in that case the mean value and boundary conditions were actually measured in the field whereas in the present case, the surface boundary needed to be assumed in most cases. The boundary was assumed based on apparent antecedent rainfall (or lack thereof) in the interval. Subsequent analysis comparing this assumption to the recorded rainfall record revealed that this assumption was valid about 56% of the time. Thus, in 44% of the cases, the surface boundary that was used in the profile development was incorrect. However, further analysis comparing the entropy profiles to those developed in the rain fed model revealed that the ALEXI profiles converged to within 0.1 in volumetric soil moisture by the bottom of the first soil layer (below the surface layer). Thus, 29% of the profiles input to DSSAT from ALEXI contained errors in volumetric soil moisture greater than 0.1 (compared to the imperfect rain fed model) in the lower soil layers. It is very difficult to determine the error this would introduce into the yield results because the amount of moisture withdrawn by the plants in a given soil layer is a function of the root factor in the DSSAT model.

The ultimate measure of the overall error in the approach is the comparison of model and observed yields. The RMSE of the modeled results represented 28% of the mean of the observations while the model exhibited a 4.7% positive bias in yield prediction. Given the various accommodations that were made as described above, these results would appear to offer evidence that the overall approach recommended here does hold promise as a means of crop simulation and forecasting in areas of scarce precipitation measurements.

6. Conclusions

In this study, a two source energy balance model, Atmospheric Land Exchange Inverse (ALEXI), based on thermal infrared remote sensing was utilized to estimate total root zone soil moisture over an agricultural region of the Southeastern U.S. and the resulting profiles were employed to drive a crop simulation model in lieu of precipitation data. Although ALEXI data were available at irregular intervals due to cloud constraints, which also led to occasional spurious readings, the results indicate that the data were available at sufficient temporal resolution to drive the crop model in a realistic manner when compared to both the rainfed model and observed corn yields (RMSE 28% of mean observed values; bias 4.7%). This result is particularly significant in that corn is the most water intensive crop grown in the Southeastern United States [72]. The comparison of ALEXI driven yields to observed yields also illustrates that the ALEXI signal did possess the fidelity to drive the crop model in a manner that was representative of the regional crop response.

The study also represents the first successful application of the principle of maximum entropy derived soil moisture profiles. Although the procedure was developed in order to employ remotely sensed data, it had only heretofore been tested in laboratory or tightly controlled field experiments [59,60,61]. The weakness of the application in this case associated with the unavailability of summer surface observations needed as a boundary condition on the profile might be overcome in future through the assimilation of microwave data with the TIR signal in order to obtain near surface soil moisture estimates.

Finally, the study demonstrated that a standard crop model, Decision Support System for Agrotechnology (DSSAT), could be reformulated to run directly with soil moisture observations in cases where precipitation data are scarce or unavailable. Since at present, remotely sensed soil moisture estimates are more readily available and reliable than are precipitation estimates from remote sensing, the results indicate that crop simulations and forecasting can be accomplished in areas with limited rainfall data.

Acknowledgements

This research project was supported by National Oceanic and Atmospheric Administration GOES–R Research Grant DG133E11SE2042 and by National Science Foundation/United States Department of Agriculture Grant 2011-67004-30334. The authors would also like to express their appreciation to the four anonymous referees and to the editor for their very helpful comments.

Conflicts of Interest

The author declares no conflict of interest.

References

1. Wood, S.J.; Jones, D.A.; Moore, R.J. Accuracy of rainfall measurement for scales of hydrological interest. *Hydrol. Earth Syst. Sci. Discuss.* **2000**, *4*, 531–543
2. Levizzani, V., Bauer, P., Turk, J., Eds. *Measuring Precipitation from Space, Advances in Global Change Research*; Springer Publishers: Amsterdam, The Netherlands, 2007; Volume 28, p. 223.
3. Simpson, J.; Kummerow, C.; Tao, W.K.; Adler, R.F. On the tropical rainfall measuring mission (TRMM). *Meteorol. Atmos. Phys.* **1996**, *60*, 19–36.
4. Arkin, P.A.; Meisner, B.N. The relationship between large-scale convective rainfall and cold cloud over the western hemisphere during 1982–84. *Mon. Wea. Rev.* **1987**, *115*, 51–74.
5. Scofield, R.A.; Naimeng, L. The Use of Satellite Imagery during the Great Floods of 1993. In Proceedings of 7th Conference Satellite Meteorology and Oceanography, Monterey, CA, USA, 6–10 June 1994; pp. 345–350.
6. Lovejoy, S.; Austin, G.L. The delineation of rain areas from visible and IR satellite data for GATE and mid-latitudes. *Atmos.-Ocean* **1979**, *17*, 77–92.
7. Gebregiorgis, A.S.; Tian, Y.; Peters-Lidard, C.; Hossain, F. Tracing hydrologic model simulation error as a function of satellite rainfall estimation bias components and land use and land cover conditions. *Water Resour. Res.* **2012**, *48*, W11509.
8. Joyce, R.J.; Xie, P. Kalman filter-based CMORPH. *J. Hydrometeorol.* **2011**, *12*, 1547–1563.

9. Sorooshian, S.; Hsu, K.L.; Gao, X.; Gupta, H.V.; Imam, B.; Braithwaite, D. Evaluation of PERSIANN system satellite based estimates of tropical rainfall. *Bull. Am. Meteorol. Soc.* **2000**, *81*, 2035–2046.
10. Hong, Y.; Adler, R.F.; Hossain, F.; Curtis, S.; Huffman, G.J. A first approach to global runoff simulation using satellite rainfall estimation. *Water Resour. Res.* **2007**, *43*, W08502.
11. Hsu, K.; Behrangi, A.; Imam, B.; Sorooshian, S. Extreme Precipitation Estimation Using Satellite-Based PERSIANN-CCS Algorithm. *Satellite Rainfall Applications for Surface Hydrology*; Gebremichael, M., Hossain, F., Eds.; Springer: New York, NY, USA, 2010.
12. Ulaby, F.T.; Dubois, P.C.; Zyl, J.V. Radar mapping of surface soil moisture. *J. Hydrol.* **1996**, *184*, 57–84.
13. Reichle, R.H.; Crow, W.T.; Keppenne, C.L. An adaptive ensemble Kalman filter for soil moisture data assimilation. *Water Resour. Res.* **2008**, *44*, W03423.
14. Anderson, M.C.; Norman, J.M.; Mecikalski, J.R.; Otkin, J.A.; Kustas, W.P. A climatological study of evapotranspiration and moisture stress across the continental United States based on thermal remote sensing: 1. Model formulation. *J. Geophys. Res.* **2007**, *112*, D10117.
15. Norman, J.M.; Kustas, W.P.; Humes, K.S. Source approach for estimating soil and vegetation energy fluxes in observations of directional radiometric surface temperature. *Agric. For. Meteorol.* **1995**, *77*, 263–293.
16. Anderson, M.C.; Hain, C.; Wardlow, B.; Pimstein, A.; Mecikalski, J.R.; Kustas, W.P. Evaluation of drought indices based on thermal remote sensing of evapotranspiration over the continental United States. *J. Climate* **2011**, *24*, 2025–2044.
17. Anderson, M.C.; Norman, J.M.; Diak, G.R.; Kustas, W.P.; Mecikalski, J.R. A two-source time-integrated model for estimating surface fluxes using thermal infrared remote sensing. *Remote Sens. Environ.* **1997**, *60*, 195–216.
18. Jones, J.W.; Hoogenboom, G.; Porter, C.H.; Boote, K.J.; Batchelor, W.D.; Hunt, L.A.; Wilkens, P.W.; Singh, U.; Gijsman, A.J.; Ritchie, J.T. The DSSAT cropping system model. *Eur. J. Agron.* **2003**, *18*, 235–265.
19. Clapp, R.B.; Hornberger, G.M. Emperical equations for some soil hydraulic properties. *Water Resour. Res.* **1978**, *14*, 601–604.
20. Twarakavi, N.K.C.; Sakai, M.; Simunek, J. An objective analysis of the dynamic nature of field capacity. *Water Resour. Res.* 2009, 45, W10410.
21. Cruise, J.F.; Arora, K. A hydroclimatic application strategy for the Poisson partial duration model. *J. Am. Water Resour. Assoc.* **1990**, *26*, 431–442.
22. Anderson, M.C.; Norman, J.M.; Mecikalski, J.R.; Otkin, J.A.; Kustas, W.P. A climatological study of evapotranspiration and moisture stress across the continental United States based on thermal remote sensing: 2. Surface moisture climatology. *J. Geophys. Res.* **2007**, *112*, D11112.
23. Anderson, M.C.; Norman, J.M.; Kustas, W.P.; Li, F.; Prueger, J.H.; Mecikalski, J.R. Effects of vegetation clumping on two–source model estimates of surface energy fluxes from an agricultural landscape during SMACEX. *J. Hydrometeorol.* **2005**, *6*, 892–909.
24. Kustas, W.P.; Norman, J.M. Evaluation of soil and vegetation heat flux predictions using a simple two-source model with radiometric temperatures for partial canopy cover. *Agric. For. Meteorol.* **1999**, *94*, 13–29.

25. Kustas, W.P.; Norman, J.M. Reply to comments about the basic equations of dual-source vegetation-atmosphere transfer models. *Agric. For. Meteorol.* **1999**, *94*, 275–278
26. Kustas, W.P.; Norman, J.M. Evaluating the effects of subpixel heterogeneity on pixel average fluxes. *Remote Sens. Environ.* **2000**, *74*, 327–342.
27. Kustas, W.P.; Norman, J.M. A two-source energy balance approach using directional radiometric temperature observations for sparse canopy covered surfaces. *Agron. J.* **2000**, *92*, 847–854.
28. Priestley, C.H.B.; Taylor, R.J. On the assessment of surface heat flux and evaporation using large-scale parameters. *Mon. Wea. Rev.* **1972**, *100*, 81–92.
29. Agam, N.; Kustas, W.P.; Anderson, M.C.; Norman, J.M.; Colaizzi, P.D.; Prueger, J.H. Application of the Priestley-Taylor approach in a two-source surface energy balance model. *J. Hydrometeorol.* **2010**, *11*, 185–198
30. Santanello, J.A.; Friedl, M.A. Diurnal variation in soil heat flux and net radiation. *J. Appl. Meteorol.* **2003**, *42*, 851–862.
31. Norman, J.M.; Divakarla, M.; Goel, N.S. Algorithms for extracting information from remote thermal-IR observations of the Earth's surface. *Remote Sens. Environ.* **1995**, *51*, 157–168.
32. Mecikalski, J.R.; Diak, G.R.; Anderson, M.C.; Norman, J.M. Estimating fluxes on continental scales using remotely sensed data in an atmospheric–land exchange model. *J. Appl. Meteorol.* **1999**, *38*, 1352–1369.
33. Carlson, T.N.; Dodd, J.K.; Benjamin, S.G.; Cooper, J.N. Satellite Estimation of the Surface Energy Balance, Moisture Availability and Thermal Inertia. *J. Appl. Meteorol.* **1981**, *20*, 67–87.
34. Norman, J.M.; Anderson, M.C.; Kustas, W.P.; French, A.N.; Mecikalski, J.; Torn, R.; Diak, G.R.; Schmugge, T.J.; Tanner, B.C.W. Remote sensing of surface energy fluxes at 101-m pixel resolutions. *Water Resour. Res.* **2003**, *39*, 1221.
35. Kustas, W.P.; Diak, G.R.; Norman, J.M. Time Difference Methods for Monitoring Regional Scale Heat Fluxes with Remote Sensing. In *Land Surface Hydrology, Meteorology, and Climate: Observations and Modeling*; Lakshmi, V., Albertson, J., Schaake, J., Eds.; AGU: Washington, DC, USA, 2001; Volume 3, pp. 15–29.
36. McNaughton, K.G.; Spriggs, T.W. A mixed-layer model for regional evaporation. *Bound.-Lay. Meteorol.* **1986**, *34*, 243–262.
37. Hain, C.R.; Crow, W.T.; Mecikalski, J.R.; Anderson, M.C.; Holmes, T. An intercomparison of available soil moisture estimates from thermal infrared and passive microwave remote sensing and land surface modeling. *J. Geophys. Res.* **2011**, *116*, D15107.
38. Otkin, J.A.; Anderson, M.C.; Mecikalski, J.R.; Diak, G.R. Validation of GOES-based insolation estimates using data from the United States Climate Reference Network. *J. Hydrometeorol.* **2005**, *6*, 460–475
39. Michalakes, J.; Dudhia, J.; Gill, D.; Henderson, T.; Klemp, J.; Skamarock, W.; Wang, W. The Weather Research and Forecast Model: Software Architecture and Performance. In Proceedings of the Eleventh ECMWF Workshop on the Use of High Performance Computing in Meteorology, Reading, UK, 25–29 October 2004; Zwieflhofer, W., Mozdzynski, G., Eds.; World Scientific: Hackensack, NJ, USA, 2005; pp. 156–168

40. Hansen, M.C.; Defries, R.S.; Townshend, J.R.G.; Sohlberg, R. Global land cover classification at 1 km spatial resolution using a classification tree approach. *Int. J. Remote Sens.* **2000**, *21*, 1331–1364.
41. Hain, C.R.; Mecikalski, J.R.; Anderson, M.C. Retrieval of an available water-based soil moisture proxy from thermal infrared remote sensing. Part I: Methodology and validation. *J. Hydrometeorol.* **2009**, *10*, 665–683.
42. Crow, W.T.; Zhan, X. Continental-scale evaluation of remotely-sensed soil moisture products. *IEEE Geosci. Remote Sens. Lett.* **2007**, *4*, 451–455.
43. Tsuji, G., Hoogenboom, G., Thornton, P., Eds.; *Understanding Options for Agricultural Production*; Kluwer Academic Publishers: Boston, MA, USA, 1998; p. 399.
44. Hoogenboom, G.; Jones, J.W.; Wilkens, P.W.; Porter, C.H.; Batchelor, W.D.; Hunt, L.A.; Boote, K.J.; Singh, U.; Uryasev, O.; Bowen, W.T.; *et al*. *Decision Support System for Agrotechnology Transfer Version 4.0*; University of Hawaii: Honolulu, HI, USA, 2004; [CD-ROM].
45. Zhang, H.; Oweis, T. Water–yield relations and optimal irrigation scheduling of wheat in the Mediterranean region. *Agr. Water Manage.* **1999**, *38*, 195–211.
46. Guereña, A.; Ruiz-Ramos, M.; Díaz-Ambrona, C.H.; Conde, J.R.; Mínguez, M.I. Assessment of climate change and agriculture in Spain using climate models. *Agron. J.* **2001**, *93*, 237–249.
47. Lopez-Cedron, F.X.; Boote, K.J.; Pineiro, J.; Sau, F. Improving the CERES-maize model ability to simulate water deficit impact on maize production and yield components. *Agron. J.* **2008**, *100*, 296–307.
48. Garcia y Garcia, A.; Hoogenboom. G.; Guerra, L.C.; Paz, J.O.; Fraisse, C.W. Analysis of the interannual variation of peanut yield in Georgia using a dynamic crop simulation model. *Trans. Amer. Soc. Agric. Biol. Eng*. **2006**, *49*, 2005–2015.
49. McNider, R.T.; Christy, J.R.; Moss, D.; Doty, K.; Handyside, C.; Limaye, A.S.; Garcia y Garcia, A.; Hoogenboom, G. A real-time gridded crop model for assessing spatial drought stress on crops in the Southeastern United States. *J. Appl. Meteorol.* **2011**, *50*, 1459.
50. Ellenburg, W.L.; Cruise, J.F.; McNider, R.T. Assessment and Mitigation of Agricultural Drought and Water Availability in the Southeastern United States Using Space Science Technology. In Proceedings of 63rd International Astronautical Congress, Naples, Italy, 1–5 October 2012; paper number IAC-12-B5.2.3, p.13.
51. Heinemann, A.B.; Hoogenboom, G.; de Faria, R.T. Determination of spatial water requirements at county and regional levels using crop models and GIS: An example for the state of Parana, Brazil. *Agr. Water Manage.* **2002**, *52*, 177–196.
52. Fang, H; Liang, S; Hoogenboom, G. Corn yield estimation through assimilation of remotely sensed data into the CSM CERES Maize model. *J. Remote Sens.* **2008**, *29*, 3011–3032.
53. Fang, H.S.; Hoogenboom, G. Integration of MODIS LAI and vegetation index products with the CSM–CERES–Maize model for corn yield estimation. *Int. J. Remote Sens.* **2011**, *32*, 1039–1065.
54. Gijsman, A.J.; Thornton, P.K.; Hoogenboom, G. Using the WISE database to parameterize soil inputs for crop simulation models. *Comput. Electron. Agric.* **2007**, *56*, 85–100.
55. White, J.W.; Hoogenboom, G.; Kimball, B.A.; Wall, G.W. Methodologies for simulating impacts of climate change on crop production. *Field Crop. Res.* **2011**, *124*, 357–368.

56. Howell, T.; Evett, S. The Penman-Monteith Method, Section 3. In *Evapotranspiration*; Determination of consumptive use in water rights: Denver, CO, USA, 2004.
57. Ritchie, J.T.; Porter, C.H.; Judge, J.; Jones, J.W.; Suleiman, A.A. Extension of an existing model for soil water evaporation and redistribution under high water content conditions. *Soil. Sci. Soc. Amer. J.* **2009**, *73*, 792–801.
58. Kostov, K.G.; Jackson, T.J. Estimating profile soil moisture from surface layer measurements. A review. *Proc. SPIE* **1993**, *1941*, 125–136.
59. Al-Hamdan, O.Z.; Cruise, J.F. Soil moisture profile development from surface observations by principle of maximum entropy. *J. Hydrol. Eng.* **2010**, *15*, 327–337.
60. Singh, V.P. Entropy theory for movement of moisture in soils. *Water Resour. Res.* **2010**, *46*, W03516.
61. Singh, V.P. Hydrologic synthesis using entropy theory: Review. *J. Hydrol. Eng.* **2011**, *16*, 421–433.
62. Jaynes E.T. Information theory and statistical mechanics. *Phys. Rev.* **1957**, *106*, 620–630.
63. Jaynes E.T. Information theory and statistical mechanics. II. *Phys. Rev.* **1957**, *108*, 171–190.
64. Chiu, C. Entropy and probability concepts in hydraulics. *J. Hydraul. Eng.* **1987**, *113*, 583–599.
65. Shannon, C.E. A mathematical theory of communication. *Bell Syst. Tech. J.* **1948**, *27*, 379–423.
66. Barbé, D.; Cruise, J.; Singh, V. Solution of Three-Constraint Entropy–Based Velocity Distribution. *J. Hydraul. Eng.* **1991**, *117*, 1389–1396.
67. Ek, M.B.; Mitchell, K.E.; Lin, Y.; Rogers, E.; Grummann, P.; Koren, V.; Gayno, G.; Tarpley, J.D. Implementation of Noah land surface model advances in the national centers for environmental prediction operational mesoscale Eta model. *J. Geophys. Res.* **2003**, *108*, doi:10.1029/2002JD003296.
68. Kumar, S.V.; Peters-Lidard, C.D.; Tian, Y.; Houser, P.R.; Geiger, J.; Olden, S.; Lighty, L.; Eastman, J.L.; Doty, B.; Dirmeyer, P.; *et al*. Land information system: An interoperable framework for high-resolution land surface modeling. *Environ. Model. Softw.* **2006**, *21*, 1402–1415.
69. Peters-Lidard, C.D.; Houser, P.R.; Tian, Y.; Kumar, S.V.; Geiger, J.; Olden, S.; Lighty, L.; Doty, B.; Dirmeyer, P.; Adams, J.; *et al.* High-performance Earth system modeling with NASA/GSFC's Land Information System. *Innov. Syst. Softw. Eng.* **2007**, *3*, 157–165.
70. National Resources Conservation Service (NRCS). *Urban Hydrology for Small Watersheds*; Technical Release 55; Conservation Engineering Division, Soil Conservation Service, US Dept. of Agriculture: Washington, DC, USA, 1986.
71. Silveira, L.; Charbonnier, F.; Genta, J.L. The antecedent soil moisture condition of the curve number procedure. *Hydrol. Sci.* **2000**, *45*, 3–12.
72. Paudel, K.; Limaye, A.; Hatch, U.; Cruise, J.; Musleh, F. Development of an optimal water allocation decision tool for the major crops during the water deficit period in the Southeast U.S. *Nat. Resour. Model.* **2005**, *18*, 281–306.